Pergamon

Int. J. Solids Structures Vol. 34, No. 1, pp. 79–98, 1997

0020–7683/97 $15.00 + .00

0020–7683(95)00291–X

ANTI-PLANE SHEAR DEFORMATIONS OF ANISOTROPIC SANDWICH STRUCTURES: END EFFECTS

S. C. BAXTER and C. O. HORGAN
Department of Applied Mathematics, School of Engineering and Applied Science, University of Virginia, Charlottesville, VA 22903, U.S.A.

(*Received* 17 *June* 1995; *in revised form* 20 *November* 1995)

Abstract—Saint-Venant decay lengths for self-equilibrated edge loads in symmetric sandwich structures are examined in the context of anti-plane shear for linear anisotropic elasticity. The most general anisotropy consistent with a state of anti-plane shear is considered. Anti-plane or longitudinal shear deformations are one of the simplest classes of deformations in solid mechanics. The resulting deformations are completely characterized by a single out-of-plane displacement that depends only on the in-plane coordinates. In linear elasticity, Saint-Venant's principle is used to show that self-equilibrated loads generate local stress effects that decay away from the loaded end of a structure. For homogeneous isotropic linear elastic materials this is well-documented. Self-equilibrated loads are a class of load distributions that are statically equivalent to zero, i.e., have zero resultant force and moment. When Saint-Venant's principle is valid, pointwise boundary conditions can be replaced by more tractable resultant conditions. It is shown in the present study that material inhomogeneity and anisotropy significantly affects the practical application of Saint-Venant's principle to sandwich structures. Copyright © 1996 Elsevier Science Ltd

1. INTRODUCTION

Anti-plane or longitudinal shear deformations are one of the simplest classes of deformations in solid mechanics. The resulting deformations are completely characterized by a single out-of-plane displacement that depends only on the in-plane coordinates. While these deformations have received little attention compared with the plane problems of linear elasticity, they have recently been investigated by Horgan and Miller (1994) in the context of anisotropic and inhomogeneous linear elasticity. A comprehensive review of *anti-plane shear* for both linear and nonlinear elasticity has been given recently by Horgan (1995).

It is the objective of the present work to utilize the relative analytic simplicity of the anti-plane shear (APS) problem to analyze Saint-Venant decay rates for self-equilibrated edge loads applied to symmetric sandwich structures. The most general anisotropy consistent with APS is considered. The cases of perfect and imperfect bonding at the layer interfaces are investigated and their effects on the stress decay rate are examined.

Designers of composite structures are constantly faced with the task of assessing stress decay effects associated with loading conditions, cut-outs, and other local discontinuities. Thus, a thorough understanding of Saint-Venant's principle as it applies to composite materials is of fundamental importance in expanding the development of composite structures technology. Previous work has shown that, even for *homogeneous* anisotropic materials, anisotropy can significantly affect the decay of Saint-Venant end effects. In particular, for the strongly anisotropic materials used in fiber-reinforced structural laminates, it has been shown that the *decay length* can be much longer than that for isotropic materials under the same loading conditions. The implications for the mechanics of composites have been widely discussed (see, e.g., the references cited at the end of the present paper).

The effects of material *inhomogeneity* have also been investigated, though not as extensively. In Choi and Horgan (1978) plane deformations of sandwich strips, with isotropic phases, were examined. In particular, for a sandwich strip with a relatively compliant core, the characteristic stress decay length is shown to be *much greater than* that for the homogeneous isotropic strip. An asymptotic estimate for the decay rate is also presented

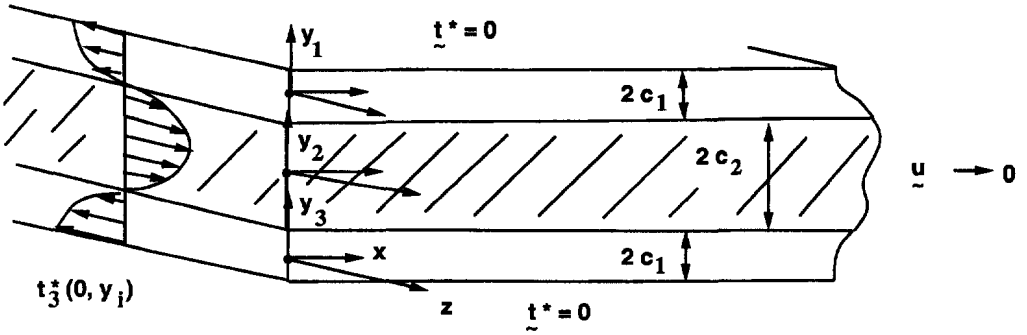

Fig. 1. Typical cross-section of symmetric sandwich structure; self-equilibrated loads applied at $x = 0$.

in Choi and Horgan (1978) which agrees well with exact numerical results (see, e.g., Horgan (1982)). See also Wijeyewickrema (1995), Wijeyewickrema and Keer (1994), and Wijeyewickrema *et al.* (1996) for more recent results on the plane problem.

In Section 2 the anti-plane shear problem is formulated for a linearly elastic sandwich structure with anisotropic phases, subject to self-equilibrated end loading only. Solutions which decay in the longitudinal direction are described and transcendental equations obtained for an eigenvalue λ on which the characteristic decay length predominantly depends. In Section 3, the special case of a sandwich structure with *isotropic* phases is examined. For this case the decay length is proportional to the half-width of the sandwich divided by λ. Asymptotic estimates for the decay length are obtained for the cases of a relatively compliant and relatively rigid core, respectively. Only one dimensionless material parameter δ, the ratio of the shear moduli of the two materials, appears in the analysis. These estimates are compared to the exact values obtained by numerical methods. Section 4 considers the effect of incorporating conditions of imperfect bonding at the layer interfaces into the model. The fully anisotropic problem is considered in Section 5. Illustrative examples for sandwich structures with *orthotropic* phases are examined in Section 6. In Section 7, the main results are summarized.

2. FORMULATION OF THE ANTI-PLANE SHEAR PROBLEM

2.1. *Geometry and kinematics*

Consider a three-layered symmetric sandwich structure with cross-section as shown in Fig. 1. The outer layers are constructed of the same material and the inner core of a second material. The material in each layer is assumed to be homogeneous, anisotropic and *linearly elastic*. The cross-section of the structure is taken to be semi-infinite. It is convenient to establish a coordinate system for each layer, with common x and z axes and separate y-axes for each layer, which are then denoted by y_1, y_2, y_3. The layers are numbered from top to bottom, 1, 2, and 3.

To study Saint-Venant end-effects in anti-plane shear, a prescribed traction of the form $\mathbf{t}^* = (0, 0, t_3^*)$, shown schematically in Fig. 1, is applied on the portion of the boundary where $x = 0$. This shear is in the direction parallel to the z-axis and independent of the out-of-plane coordinate z, i.e., $t_3^* = t_3^*(0, y_i)$. The top and bottom surfaces of the sandwich are taken to be traction-free, and the applied tractions at $x = 0$ are assumed to be *self-equilibrated*. As $x \to \infty$, it is assumed that $\mathbf{u} = (u_1, u_2, u_3) \to 0$. Under such conditions it is shown by Horgan and Miller (1994) that the deformation is an *anti-plane shear* (APS) deformation with

$$u_1 = 0, \quad u_2 = 0, \quad u_3 = u_3(x, y_i). \tag{1}$$

Since the out-of-plane displacement is the only non-zero component of displacement, the subscript 3 will be dropped where convenient, and u^i will signify the displacement in the i^{th}

layer. The constitutive equation for an anisotropic linearly elastic solid is used, i.e., the generalized Hooke's law

$$T_{ij} = C_{ijkl}\varepsilon_{kl}, \tag{2}$$

where T_{ij} are the Cauchy stress components and ε_{kl} are the linear strains. The C_{ijkl} are the elastic coefficients; for each homogeneous layer they are constants, and satisfy the usual symmetry conditions. It is shown by Horgan and Miller (1994) that the conditions

$$C_{\alpha\beta 3\gamma} \equiv 0, \quad (\alpha, \beta, \gamma = 1, 2) \quad \text{in each layer} \tag{3}$$

are *sufficient* for a non-trivial (i.e., grad $u_3 \neq 0$), state of APS to be sustained in the body. The out-of-plane displacement $u_3 \equiv u$ must then satisfy the single equation

$$C_{3\beta 3\alpha}u_{,\alpha\beta} = 0 \quad \text{on} \quad \mathscr{D}, \tag{4}$$

where $\mathscr{D}$ denotes the cross-section of the composite. As discussed by Horgan and Miller (1994), a wide class of anisotropic materials, including the monoclinic material (with 13 independent elastic constants) satisfy (3).

Using the notation

$$C_{3\beta 3\alpha} \equiv A_{\alpha\beta}, \quad A_{\alpha\beta} = A_{\beta\alpha}, \tag{5}$$

eqn (4) can be rewritten as

$$A_{\alpha\beta}u_{,\alpha\beta} = 0 \quad \text{on} \quad \mathscr{D}. \tag{6}$$

The non-zero in-plane stresses are

$$T_{31} = A_{11}u_{,1} + A_{12}u_{,2}, \tag{7}$$

$$T_{32} = A_{21}u_{,1} + A_{22}u_{,2}. \tag{8}$$

The three-dimensional strain energy density is assumed positive definite in each layer. This assumption requires that

$$A_{11} > 0, \quad A_{11}A_{22} - A_{12}^2 \equiv A^2 > 0, \tag{9}$$

for each layer.

It is assumed that the materials are perfectly bonded at the layer interfaces so that the displacements and tractions are continuous there, so that

$$u^1(x, -c_1) = u^2(x, c_2), \tag{10}$$

$$u^2(x, -c_2) = u^3(x, c_1), \tag{11}$$

and

$$a_{12}u^1_{,1}(x, -c_1) + a_{22}u^1_{,2}(x, -c_1) = b_{12}u^2_{,1}(x, c_2) + b_{22}u^2_{,2}(x, c_2), \tag{12}$$

$$b_{12}u^2_{,1}(x, -c_2) + b_{22}u^2_{,2}(x, -c_2) = a_{12}u^3_{,1}(x, c_1) + a_{22}u^3_{,2}(x, c_1), \tag{13}$$

respectively. In (12) and (13) the $A_{\alpha\beta}$ of eqn (6) are replaced by $a_{\alpha\beta}$, representing the material constants in layers 1 and 3, and $b_{\alpha\beta}$, representing those of layer 2.

The traction-free boundary conditions on the top and bottom read

$$a_{12}u^1_{,1}(x,c_1)+a_{22}u^1_{,2}(x,c_1)=0, \tag{14}$$

$$a_{12}u^3_{,1}(x,-c_1)+a_{22}u^3_{,2}(x,-c_1)=0. \tag{15}$$

Since they are not used explicitly, the boundary conditions at $x=0$ are not written down.

2.2. *Forms of the solution*

It is shown by Baxter (1995), and Baxter and Horgan (1995) that exponentially decaying solutions of (6) may be written as

$$u^i(x,y_i)=\exp\left[-\frac{\lambda_i}{c_i\sqrt{B_i}}x\right]\exp\left[\frac{\lambda_i}{c_i\sqrt{B_i}}\left(\frac{A_{12}}{A_{22}}\right)y_i\right] \times\left[\alpha_i\cos\left(\frac{\lambda_i}{c_i}y_i\right)+\beta_i\sin\left(\frac{\lambda_i}{c_i}y_i\right)\right],\quad i=1,2,3, \tag{16}$$

where $\lambda_i>0$, since it is required that $u^i\to 0$ as $x\to\infty$. It is understood that $c_3\equiv c_1$. The dimensionless material parameters B_i in (16) are defined by

$$B_1=B_3=\frac{a_{11}a_{22}-a_{12}^2}{a_{22}^2}, \tag{17}$$

$$B_2=\frac{b_{11}b_{22}-b_{12}^2}{b_{22}^2}. \tag{18}$$

Equation (16) represents the solution in the i^{th} layer. The α_i and β_i are constants that differ in each layer, the $A_{\alpha\beta}$ are the appropriate material coefficients; i.e., $a_{\alpha\beta}$ in layers 1 and 3, and $b_{\alpha\beta}$ in layer 2, and the c_i are the half-width of each layer. (See Fig. 1.) Because eqns (10) and (11) must hold for all x, it follows from (16) that

$$\frac{\lambda_1}{c_1\sqrt{B_1}}=\frac{\lambda_2}{c_2\sqrt{B_2}}=\frac{\lambda_3}{c_3\sqrt{B_3}}, \tag{19}$$

and so the exponential *decay rates* in (16) are the same for each layer. Since $c_1\equiv c_3$, and $B_1\equiv B_3$, we see that $\lambda_1=\lambda_3$. Introducing the notation

$$\frac{\lambda_1}{c_1\sqrt{B_1}}=\frac{\lambda_2}{c_2\sqrt{B_2}}\equiv\frac{\lambda}{2c_1\sqrt{B_1}+c_2\sqrt{B_2}}\equiv k, \tag{20}$$

the exponential decay rates $\lambda_\alpha/c_\alpha\sqrt{B_\alpha}$ can be compared with that for a homogeneous strip of "weighted" total half-width $(2c_1\sqrt{B_1}+c_2\sqrt{B_2})$. If a non-dimensional weighted volume fraction is defined as

$$\hat{f}=\frac{2c_1\sqrt{B_1}}{2c_1\sqrt{B_1}+c_2\sqrt{B_2}}, \tag{21}$$

it is possible to express both λ_1 and λ_2 in terms of λ and $\hat{f}$:

$$\lambda_1=\frac{\hat{f}\lambda}{2},\quad \lambda_2=\lambda(1-\hat{f}). \tag{22}$$

When (16) is substituted into (10)–(15), the conditions for a nontrivial solution of the

resulting linear homogeneous system of equations is a transcendental equation satisfied by λ (see Baxter (1995)), and given by

$$-\hat{\delta}^2 \sin^2(\hat{f}\lambda) \sin[2\lambda(1-\hat{f})] + \cos^2(\hat{f}\lambda) \sin[2\lambda(1-\hat{f})] + 2\hat{\delta} \cos(\hat{f}\lambda) \cos[2\lambda(1-\hat{f})] \sin(\hat{f}\lambda) = 0, \quad (23)$$

where

$$\hat{\delta} \equiv \frac{a_{22}\sqrt{B_1}}{b_{22}\sqrt{B_2}} \equiv \sqrt{\frac{a_{11}a_{22}-a_{12}^2}{b_{11}b_{22}-b_{12}^2}}. \quad (24)$$

By virtue of (9), it is seen that

$$\hat{\delta} > 0. \quad (25)$$

It is shown by Baxter (1995) that the roots λ of (23) are all real. A complete solution to (6), subject to prescribed boundary conditions at $x = 0$, would involve an infinite series of eigenfunctions of the form (16). As explained in Horgan and Knowles (1983) and Horgan (1989), for example, the *decay rate* k for the solution in each layer is given by (20), where λ is the *smallest eigenvalue*, i.e., the smallest positive root of (23). By virtue of (7), (8), k is also the decay rate for the stresses.

3. SPECIALIZATION TO ISOTROPY

If each of the layers is assumed to be *isotropic*, considerable simplification occurs. In this case the material constants in the outer layer are

$$a_{11} = a_{22} \equiv \mu_1, \quad a_{12} \equiv 0, \quad (26)$$

and so

$$B_1 = 1. \quad (27)$$

In the center core layer

$$b_{11} = b_{22} \equiv \mu_2, \quad b_{12} \equiv 0, \quad (28)$$

and thus

$$B_2 = 1. \quad (29)$$

In the above, μ_1 and μ_2 are the shear moduli of the material in the outer layers and the core, respectively. These shear moduli are the only elastic constants that appear in the analysis of the isotropic problem. Using (27), (29) and (20) the exponential decay factor e^{-kx} for each layer has a decay rate k given by

$$k = \frac{\lambda}{2c_1 + c_2}, \quad (30)$$

where λ is the smallest positive root of (23). The *characteristic decay length* d (i.e., the distance over which end effects decay to 1% of their value at $x = 0$) is defined by

$$d \equiv \frac{\ln(100)}{k}. \quad (31)$$

The weighted volume fraction, $\hat{f}$, given by (21), reduces to a simple volume fraction

$$f \equiv \frac{2c_1}{2c_1 + c_2}, \tag{32}$$

representing the relative thickness of an outer layer to the half-width of the entire structure. In what follows, primary attention will be given to f within the interval $0.1 \leqslant f \leqslant 0.9$. The ends of this interval correspond to the physical ideas of a *thin* and *thick* outer layer respectively. Similarly, the limits $f \to 0$ and $f \to 1$ correspond to a *homogeneous* strip composed of the core or face material only. For the isotropic sandwich, the material parameter $\hat{\delta}$, defined by (24), now simplifies to the ratio of the two shear moduli

$$\delta \equiv \frac{\mu_1}{\mu_2}. \tag{33}$$

The parameters without the "carat" symbol will denote the isotropic case. The form of the transcendental eqn (23) remains the same, with $\hat{f}$, $\hat{\delta}$ replaced by f, δ for the isotropic case. For convenience the parameter δ is referred to as the *core ratio*, with the understanding that a large core ratio means that the core is more compliant in shear than the outer layers and a small core ratio means that the core is stiffer in shear than the outer layers.

3.1. *Properties of the transcendental equation*

Some properties of the transcendental eqn (23) in the isotropic case are established in Baxter (1995). For convenience, these are summarized below:

1. The eigenvalues are real.
2. The transcendental equation can be factored. It will be assumed that $\lambda \neq 0, f \neq 0.5$. (When $f = 0.5$ the transcendental equation can be solved explicitly for λ, see below.) The decay rate, given by (30), is λ/(half-width of strip), where λ is the *smallest* root of the reduced equation

$$\cot(f\lambda)\cot[(1-f)\lambda] - \delta = 0. \tag{34}$$

   It can be seen that this equation is symmetric with respect to interchanges of f and $(1-f)$, so that the smallest positive root is unaffected by this exchange. Each f with its corresponding $(1-f)$ will be referred to as a symmetric pair.
3. When $\mu_1 = \mu_2$ so that the strip is homogeneous, (33) yields $\delta = 1$. In this case, eqn (23) reduces to

$$\sin(2\lambda) = 0. \tag{35}$$

   The smallest positive root of (35) yields the exact decay rate for a homogeneous isotropic strip, i.e.,

$$\lambda = \frac{\pi}{2}, \tag{36}$$

   so that u decays as

$$e^{-kx}, \quad k = \pi/h, \tag{37}$$

   where h is the strip width. The decay length is thus approximately one and a half times the strip width. The foregoing results for *harmonic* functions on semi-infinite strips are well-known (see, e.g., Horgan and Knowles (1983), Horgan (1989)).
4. Equation (23) can be solved explicitly for λ when $f = 0.5$, i.e., when $2c_1 = c_2$. This will be referred to as the canonical geometry, and the decay length is given by (31), (30) with

$$\lambda = 2\tan^{-1}\left(\frac{1}{\sqrt{\delta}}\right). \tag{38}$$

3.2. *Asymptotic estimates as* $\delta \to \infty$

Analogous work on the plane problem by Choi and Horgan (1978) shows that for a relatively compliant inner core ($\mu_1 \gg \mu_2$), i.e., $\delta \to \infty$, the decay length tends to infinity. Numerical solutions to (34) verifies that this is the case here also. An asymptotic analysis of (34) with (30), (31) shows that

$$\bar{d} \sim \ln(100)[\delta f(1-f)]^{1/2} \text{ as } \delta \to \infty (0 < f < 1), \tag{39}$$

where the dimensionless *scaled decay length* is defined by

$$\bar{d} \equiv \frac{d}{2c_1 + c_2}. \tag{40}$$

The exact $\bar{d}$, computed from (31), (34), (40), are shown by the solid curves in Figs 2 and 3.

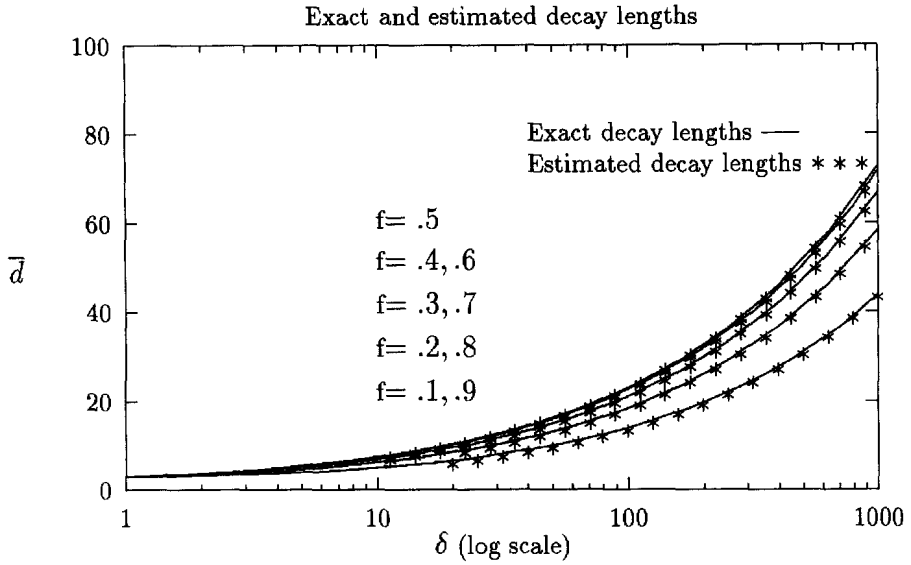

Fig. 2. Scaled decay length vs δ, for various f.

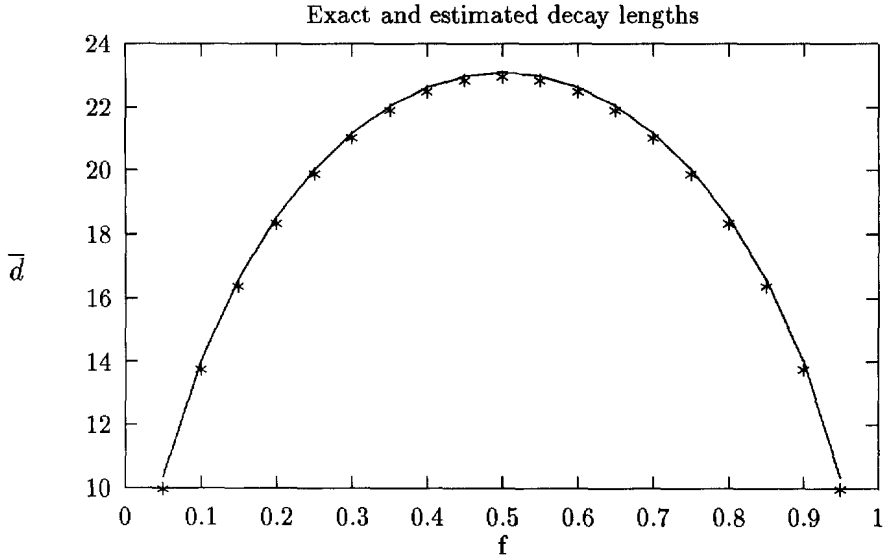

Fig. 3. Scaled decay length vs volume fraction ($\delta = 100$).

The asterisk denotes values calculated from the asymptotic formula (39). Note that the asymptotic estimate is invariant with respect to interchanges of f and $(1-f)$. Figure 2 indicates that for values of $\delta \geqslant 100$, $0.1 \leqslant f \leqslant 0.9$, the result (39) provides a very accurate estimate for the decay length.

3.3. *Asymptotic estimates as* $\delta \to 0$

It is shown by Baxter (1995) that

$$\bar{d} \doteq \begin{cases} \frac{2}{\pi}\ln(100)[(1-f)+f\delta], & (0 < f \leqslant 0.5) \\ \frac{2}{\pi}\ln(100)[f+(1-f)\delta], & (0.5 \leqslant f < 1) \end{cases} \quad \text{as } \delta \to 0. \tag{41}$$

From the definition of δ in (33), it is seen that $\delta \to 0$ corresponds to $\mu_1 \ll \mu_2$, i.e., a relatively stiff inner core. The exact decay lengths for a range of δ representing a stiff core are plotted in Fig. 4 and compared with the limiting estimate (41).

3.4. *Summary*

For the isotropic sandwich structure the decay lengths are the *same* for each symmetry pair, f and $(1-f)$, throughout the range of the core ratio. Increasing order of the symmetry pairs is defined as follows, (0.1, 0.9), (0.2, 0.8), (0.3, 0.7), (0.4, 0.6), (0.5, 0.5), the last of which is the canonical geometry.

The effect of geometry is reversed at the transition value $\delta = 1$. For a stiff core, ($\delta < 1$), decay lengths *decrease* with the *increasing* order of the symmetry pairs. For a compliant core, ($\delta > 1$), decay lengths *decrease* with the *decreasing* order of the symmetry pairs. The decay length is a monotonic *increasing* function of the core ratio δ. These results are analogous to those of Choi and Horgan (1978) for the plane problem which predict slower decay rates, and thus longer decay lengths, for an increasingly compliant core. An asymptotic result analogous to (39) is also obtained in Choi and Horgan (1978) (see eqn (4.1)). See also Horgan (1982).

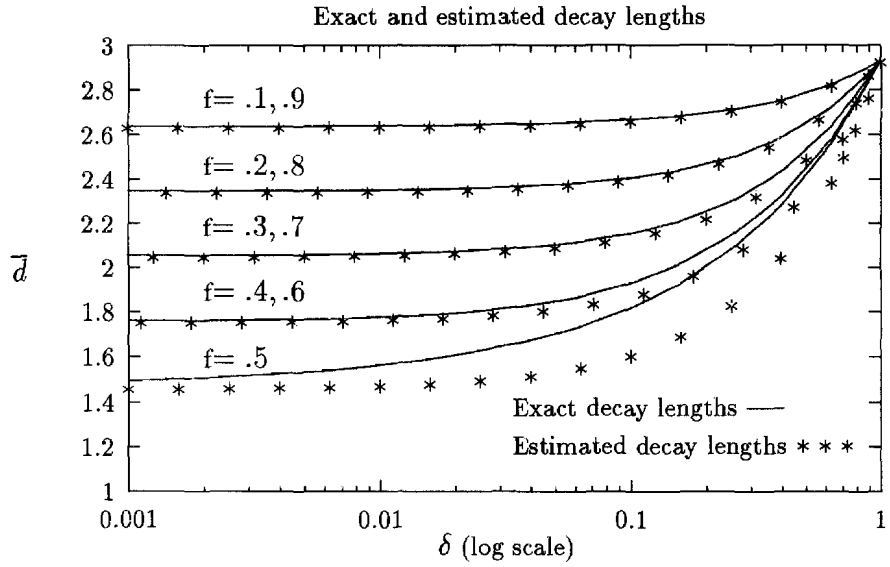

Fig. 4. Scaled decay length vs δ, for various f.

4. IMPERFECT BONDING

4.1. *Modified interfacial conditions*

The condition of perfect bonding used in Section 2 assumes that both displacements and tractions are continuous across the layer interfaces. In this section the consequences of relaxing this condition are examined. In what follows, attention will be confined to the case of *isotropic phases*. The condition of imperfect bonding (see, e.g., Benveniste (1984), Aboudi (1987)) is modeled in the anti-plane shear context by modifying the interfacial conditions to allow jumps in the displacements proportional to the tractions at the interface. In the present case, there are no normal tractions at the interfaces so these conditions refer only to the tangential displacements. It is assumed that (12) and (13), the conditions for continuous traction, with $a_{12} = 0$, $b_{12} = 0$, $a_{11} = a_{22} = \mu_1$, $b_{11} = b_{22} = \mu_2$, still hold. Equations (10) and (11) are replaced by

$$u^1(x,-c_1)-u^2(x,c_2) = \mathscr{R}T_{32}, \tag{42}$$

$$u^2(x,-c_2)-u^3(x,c_1) = \mathscr{R}T_{32}, \tag{43}$$

respectively, where $\mathscr{R}$ is a constant of proportionality and T_{32} serves to represent the components of traction at the interfaces. As $\mathscr{R} \to 0$, perfect bonding is recovered, while as $\mathscr{R} \to \infty$, perfectly lubricated contact (Aboudi (1987)) at the interfaces is obtained. It is convenient to define a new dimensionless parameter

$$\alpha \equiv \frac{(\mu_1+\mu_2)\mathscr{R}}{2c_1+c_2}. \tag{44}$$

Use of this parameter is motivated by the form of eqn (49) in Benveniste (1984) except here it is scaled by the half-width of the structure rather than the total width. On using the definition of δ in (33), this dimensionless constant can be rewritten as

$$\alpha \equiv \frac{(1+\delta)\mu_2\mathscr{R}}{2c_1+c_2}, \tag{45}$$

which will be referred to henceforth as the slip constant. When $\mathscr{R} = 0$, so that the interfaces are perfectly bonded, then it follows that $\alpha = 0$. For typical slipping interfaces, α is a small number. For example, if the core material is glass and the face material an epoxy resin, the data given in Devries (1993) on pages 361 and 366 suggest that $\alpha\,(2c_1+c_2) \doteq 3.138310^{-4}$ m.

The transcendental equation for λ is (see Baxter (1995))

$$\begin{aligned}
&\frac{\alpha^2\delta^2\lambda^2}{(1+\delta)^2}\sin^2(f\lambda)\sin[2\lambda(1-f)] - 2\frac{\alpha\delta^2\lambda}{(1+\delta)}\sin^2(f\lambda)\cos[2\lambda(1-f)] \\
&\quad -2\frac{\alpha\delta\lambda}{(1+\delta)}\sin(f\lambda)\sin[2\lambda(1-f)]\cos(f\lambda) - \delta^2\sin^2(f\lambda)\sin[2\lambda(1-f)] \\
&\quad +\cos^2(f\lambda)\sin[2\lambda(1-f)] + 2\delta\cos(f\lambda)\cos[2\lambda(1-f)]\sin(f\lambda) = 0.
\end{aligned} \tag{46}$$

As $\alpha \to 0$, (46) reduces to (23) without the carat symbol.

4.2. *Decay lengths*

The values of the scaled decay lengths $\bar{d}$ for the sandwich structure with $f = 0.5$, and for representative values of the core ratio, i.e., $\delta = 0.1$, $\delta = 0.5$, $\delta = 1$, $\delta = 2$, $\delta = 10$, are

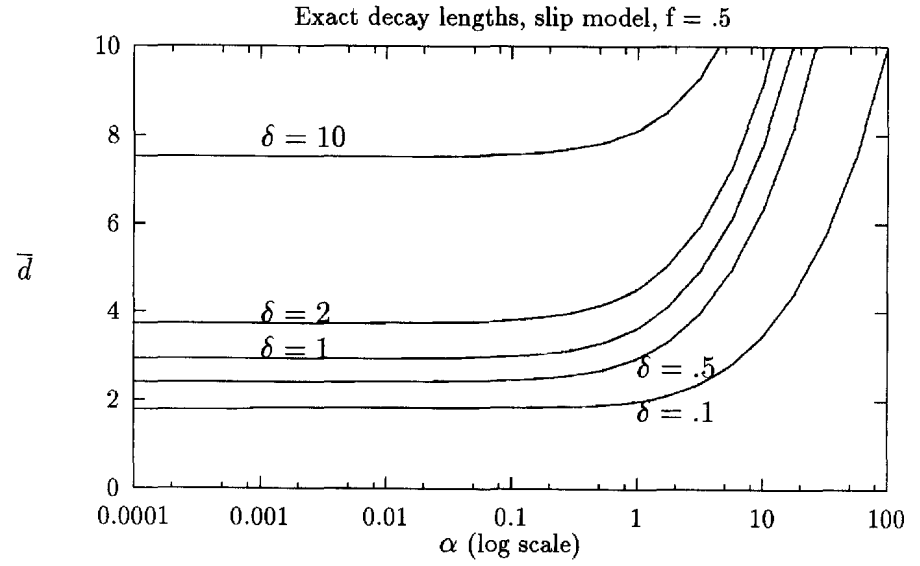

Fig. 5. Exact decay lengths vs α, volume fraction $f = 0.5$.

plotted in Fig. 5 for the range $0 \leqslant \alpha \leqslant 100$. Setting $\delta = 1$ corresponds to the physical case where, for $\alpha > 0$, layers of identical materials are allowed to slip. The case $\alpha = 0$, $\delta = 1$ corresponds to a homogeneous isotropic strip for which $\bar{d} = 2 \ln (100)/\pi$ (see (31), (36)).

Benveniste (1984) calculated the exact decay rates for a similar sandwich structure under conditions of plane strain, where imperfect bonding, i.e., discontinuous tangential displacements were allowed. The material parameter used by Benveniste (1984), which is comparable to the core ratio δ used here, is the ratio of the Young's moduli, E_1/E_2. Two values were chosen by Benveniste (1984); namely $E_1/E_2 = 2$ and $E_1/E_2 = 10$. In Figs 3 and 4 of Benveniste (1984), the exact decay rates are plotted vs

$$\bar{R} \equiv \frac{R(E_1 + E_2)}{(r_1 + r_2)(c_1 + c_2)}, \tag{47}$$

where R is the constant of proportionality used in Benveniste (1984), and the r_i involve the Poisson ratio for each layer, of width c_i, respectively (cf. (44)). The scaled decay lengths in Fig. 5 may then be compared to the scaled decay rates $\bar{k}$ plotted in Figs 3 and 4 of Benveniste (1984).

In both works, as α or $\bar{R}$ increases, the decay length increases and tends to infinity as α or $\bar{R} \to \infty$. Thus, the larger the amount of slip, the slower the attenuation of Saint-Venant end effects. The implications for the mechanics of composites, for example in estimating effective moduli, is discussed in Benveniste (1984). Under either deformation, APS or plane strain, it is seen from Fig. 5 here and Fig. 3 of Benveniste (1984), where $E_1/E_2 < 1$, that the *longer* decay length is associated with the *larger* core ratio δ (a more compliant core). Figure 4 of Benveniste (1984) shows that for the plane problem with $E_1/E_2 > 1$, this ordering is reversed in the range $1 \leqslant \bar{R} \leqslant 1000$.

4.3. *Asymptotic estimates as* $\alpha \to \infty$

The numerical results illustrated in Fig. 5 show that the decay length tends to infinity as $\alpha \to \infty$. This motivates the development of asymptotic formulas which describe this limiting behavior. It is shown in Baxter (1995) that

$$\bar{d} \sim \ln(100) \sqrt{\frac{\alpha \delta f}{(1+\delta)}} \quad \text{as} \quad \alpha \to \infty. \tag{48}$$

In Fig. 6 values calculated from the estimate (48), when $f = 0.5$, for the two values of the

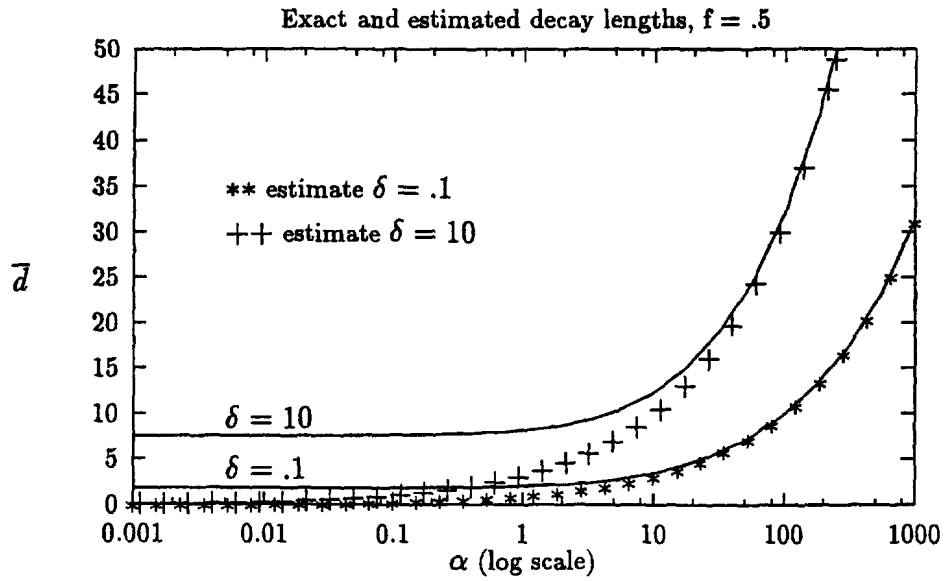

Fig. 6. Exact and estimated decay lengths vs α, volume fraction $f = 0.5$.

material parameter $\delta = 0.1$, $\delta = 10$ is denoted by asterisks. It is seen that (48) provides an accurate estimate for large values of α. From (48) it is also seen that for large values of α and all values of δ the decay lengths increase with increasing volume fraction.

4.4. *Summary*

Relaxing the interfacial conditions by allowing a jump in the tangential displacement proportional to the shear traction on the interface results in longer decay lengths than under conditions of perfect bonding. This is seen in Fig. 5, where the values of the decay length at $\alpha = 0$ correspond to the case of perfect bonding. It is also easily seen from this figure that as the amount of slip increases the decay length increases. This trend is physically intuitive in that slip between the interfaces represents a loss in the rigidity of the structure and a slower decay of end effects would then be expected. For a noticeable range of small α, the decay lengths are virtually the same as those for perfect bonding with the same core ratio and volume fraction. From Fig. 5 it is also seen that while the decay lengths increase as the slip constant α increases they also increase with increasing δ. This is the same relationship observed under conditions of perfect bonding. These points of similarity with the case of perfect bonding suggest that the addition of a small non-zero slip constant in modeling a sandwich structure preserves the material and geometric effects predicted by the perfect bonding model.

5. THE GENERAL ANISOTROPIC CASE

Under the most general anisotropy consistent with anti-plane shear, the decay rate k is given by $(20)_3$, i.e.,

$$k = \frac{\lambda}{2c_1\sqrt{B_1} + c_2\sqrt{B_2}}, \tag{49}$$

where the dimensionless material parameters B_α are defined in (17), (18) and the transcendental equation for λ is given by eqn (23). Recall from (24), (21) that the following definitions hold:

$$\hat{\delta} \equiv \sqrt{\frac{a_{11}a_{22}-a_{12}^2}{b_{11}b_{22}-b_{12}^2}}, \tag{50}$$

$$\hat{f} = \frac{2c_1\hat{\delta}}{2c_1\hat{\delta}+c_2\gamma}. \tag{51}$$

To obtain (51), eqns (17), (18) have been used and the new dimensionless material parameter

$$\gamma \equiv \frac{a_{22}}{b_{22}} \tag{52}$$

has been introduced. The two parameters $\hat{\delta}$ and γ are related to B_1 and B_2 by

$$\frac{\hat{\delta}}{\gamma} = \sqrt{\frac{B_1}{B_2}}. \tag{53}$$

The decay length d is still defined by (31). On using (49) it can be written as

$$d = \frac{\ln(100)\sqrt{B_2}}{\lambda}\left[\frac{2c_1\hat{\delta}+c_2\gamma}{\gamma}\right]. \tag{54}$$

In the case of isotropy, it was possible to reduce the number of material parameters from the original two, i.e., μ_1 and μ_2, to a single dimensionless parameter $\delta = \mu_1/\mu_2$, which is a measure of the relative magnitudes of the shear moduli in the face layers and core. In the anisotropic case, the problem as originally formulated involves six material constants. While the eigenvalue λ depends only on *two* dimensionless material parameters, namely $\hat{\delta}$ and γ, it is seen from (54) that the decay length d depends on *three* such parameters $\hat{\delta}$, γ and B_2 (or B_1). The parameters $\hat{\delta}$, γ serve as a relative measure of the properties of one material to the other. The isotropic case is recovered on setting $a_{12} = 0$, $b_{12} = 0$, $a_{11} = a_{22} = \mu_1$, $b_{11} = b_{22} = \mu_2$ in which case $\hat{\delta} \equiv \gamma = \delta$, and $B_2 = B_1 = 1$. The geometry is characterized by the volume fraction f defined in (32). On making use of (32) in (51), the quantity $\hat{f}$ can be rewritten as

$$\hat{f} = \frac{f\hat{\delta}}{f\hat{\delta}+(1-f)\gamma}. \tag{55}$$

It can be readily verified that

$$0 < \hat{f} < 1. \tag{56}$$

The quantity $\hat{f}$ is fully specified by the choice of f, $\hat{\delta}$, and γ. In the following, the geometric parameter, f, will be restricted to the interval $0.1 \leqslant f \leqslant 0.9$ and limiting values of f will again represent a thin or a thick core. In this geometric interval, the *range* of $\hat{f}$ is still $0 < \hat{f} < 1$, but $\hat{f}$ can be close to 0 or 1.

5.1. *Properties of the transcendental equation*

Some properties of eqn (23) are established in Baxter (1995):

1. The eigenvalues λ are real.
2. The transcendental eqn (23) can be factored. It will be assumed that $\lambda \neq 0, \hat{f} \neq 0.5$. When $\hat{f} = 0.5$ the transcendental equation can be solved explicitly for λ (see below). The corresponding reduced form of (23) is

$$\cot(\hat{f}\lambda)\cot[(1-\hat{f})\lambda]-\hat{\delta}=0. \tag{57}$$

Equation (57) is symmetric with respect to interchanges of $\hat{f}$ and $(1-\hat{f})$ but, as pointed out above, since $\hat{f}$ also involves material parameters, this does not represent a geometric symmetry.

3. When $\hat{\delta}=1$, eqn (23) reduces to (35), so that the eigenvalue λ is the same as that for the homogeneous isotropic strip, i.e.,

$$\lambda=\pi/2, \tag{58}$$

for all geometries. Observe that $\hat{\delta}=1$ simply requires that

$$a_{11}a_{22}-a_{12}^2=b_{11}b_{22}-b_{12}^2, \tag{59}$$

making this a special sandwich strip with anisotropic layers and core whose elastic constants are related by (59). When $\hat{\delta}=1$, it follows from (53) that

$$B_2=\gamma^2 B_1, \tag{60}$$

so that, on using (58), (54) now reads

$$d=\frac{2\ln(100)}{\pi}[\sqrt{B_1}(2c_1+\gamma c_2)]. \tag{61}$$

4. When $\hat{\delta}=\gamma$, it follows from (51) that $\hat{f}=f$. Replacing $\hat{\delta}$ by γ in (23) it is seen that the eigenvalues λ are identical to those of the *isotropic* sandwich strip if $\hat{\delta}$ in (23) is identified with γ. Observe that $\hat{\delta}=\gamma$ simply requires that

$$a_{22}^2(b_{11}b_{22}-b_{12}^2)=b_{22}^2(a_{11}a_{22}-a_{12}^2), \tag{62}$$

or equivalently

$$B_1=B_2\equiv B. \tag{63}$$

This is again a special sandwich strip where the elastic constants are related by (62). When (62) holds, (54) reads

$$d=\frac{\ln(100)}{\lambda}[\sqrt{B}(2c_1+c_2)]. \tag{64}$$

The analysis of Section 3 for λ can now be applied in the present case with δ in Section 3 replaced by γ defined in (52). The decay length d has a further dependence on the elastic constants through the appearance of $\sqrt{B}$ in (64).

5. When $a_{\alpha\beta}\equiv b_{\alpha\beta}$ so that the strip is homogeneous, $\hat{\delta}=1$, $\gamma=1$ and again $B_1=B_2\equiv B$. In this case (23) reduces to

$$\sin(2\lambda)=0, \tag{65}$$

so that

$$\lambda=\frac{\pi}{2} \tag{66}$$

(cf. (36) in the isotropic case). Thus the decay length is

$$d = \frac{\ln(100)}{\pi}\sqrt{B}h = \frac{\ln(100)}{\pi}\left(\frac{\sqrt{a_{11}a_{22}-a_{12}^2}}{a_{22}}\right)h, \tag{67}$$

where h is the strip width. The result (67) was obtained previously in Horgan and Payne (1993) and Horgan and Miller (1994). The isotropic result follows from (67) on setting $a_{12} = 0$, $a_{11} = a_{22}$.

6. Equation (23) can be solved explicitly for λ when $\hat{f} = 0.5$. This will be called the anisotropic canonical case. In this case, on using (55), the volume fraction f and the material parameters $\hat{\delta}$, γ are related by

$$\frac{f}{(1-f)} = \frac{\gamma}{\hat{\delta}}. \tag{68}$$

The smallest positive root λ for the anisotropic canonical case is given by

$$\lambda = 2\tan^{-1}\left(\frac{1}{\sqrt{\hat{\delta}}}\right). \tag{69}$$

This is the anisotropic analog of (38). The decay length is given by (54), with λ as in (69).

7. In the case where each of the layers is constructed of an *orthotropic* material, i.e., when

$$a_{12} = 0, \quad b_{12} = 0, \tag{70}$$

the material parameters simplify slightly, so that

$$\hat{\delta} = \sqrt{\frac{a_{11}a_{22}}{b_{11}b_{22}}}, \quad \gamma = \frac{a_{22}}{b_{22}}, \tag{71}$$

$$\sqrt{B_1} = \sqrt{\frac{a_{11}}{a_{22}}}, \quad \sqrt{B_2} = \sqrt{\frac{b_{11}}{b_{22}}}. \tag{72}$$

In the special subcase where the structure is composed of the *same* orthotropic material, with the core layer rotated 90° off the original material axis, then the structure behaves as if it is composed of two *different* orthotropic materials. When the x-axis coincides with the principal material axis,

$$a_{11} = G_{31}, \quad a_{22} = G_{32}, \tag{73}$$

and when the material is rotated 90°, the core moduli are then

$$b_{11} = G_{32}, \quad b_{22} = G_{31}. \tag{74}$$

In each case the shear moduli G_{31} and G_{32} are given with respect to a fixed material orientation. From (71), it is now seen that $\hat{\delta} = 1$ for all geometries so that this case is a subcase of 3 above and λ is given by (66). From (72)

$$\sqrt{B_1} = \frac{1}{\sqrt{B_2}} = \sqrt{\frac{G_{31}}{G_{32}}} \equiv \omega, \tag{75}$$

where ω is a new dimensionless material parameter. Further discussion of this special case is carried out in the next section.

6. ORTHOTROPIC LAYERS

When the layers of the sandwich structure are constructed of orthotropic materials, then $\hat{\delta}$, γ, B_α are given by (71), (72), and the decay length is given by (54). The decay length depends on three material parameters $\hat{\delta}$, γ, and $\sqrt{B_1}$ or $\sqrt{B_2}$. Two illustrative examples are considered below. In the first example, the same orthotropic material is used in two orientations, while in the second, specific numerical data is used for two independent orthotropic materials.

6.1. [0/90/0] *Orthotropic structure*

A sandwich structure is constructed of one orthotropic material. In layers 1 and 3, the main axis of the material lies parallel to the x-axis. In layer 2, the main axis of the material lies parallel to the structure's z-axis. For this structure the material constants are given by (73) and (74). On using (66) and (75) in (54), the decay length d now reads

$$d = \frac{2\ln(100)}{\pi}\left[2c_1\omega + \frac{c_2}{\omega}\right], \tag{76}$$

which depends on the single material parameter ω. From (76) it is seen that

$$d \to \infty, \quad \text{as } \omega \to 0, \tag{77}$$

$$d \to \infty, \quad \text{as } \omega \to \infty, \tag{78}$$

so that the decay length tends to infinity for both limiting cases. The decay lengths for this structure will be compared below to those for the homogeneous isotropic strip and for the isotropic two phase structure, which also depends on only one material parameter.

It is easy to show from (76) that, for a given geometry, the minimum decay length occurs when

$$\omega = \sqrt{\frac{(1-f)}{f}}. \tag{79}$$

Substituting (79) into (76), the minimum decay length is then explicitly given as

$$d_{\min} = \ln(100)\left(\frac{4}{\pi}\right)\sqrt{2c_1c_2}. \tag{80}$$

To plot the decay length for a variety of geometries, it is again convenient to use the scaled decay length as in (40) so that

$$\bar{d} = \frac{2\ln(100)}{\pi}\left[f\omega + \frac{(1-f)}{\omega}\right], \tag{81}$$

and thus

$$\bar{d}_{\min} \equiv \frac{4\ln(100)}{\pi}[\sqrt{f(1-f)}]. \tag{82}$$

Figure 7 plots $\bar{d}$ vs ω for various volume fractions in the range $0.1 \leqslant f \leqslant 0.9$.

Orthotropic two phase vs homogeneous isotropic strip. The degree of applicability of Saint-Venant's principle for this structure is assessed by comparing the orthotropic scaled decay length to the scaled decay length of a homogeneous isotropic strip. Thus, when

$$\bar{d} = \frac{2\ln(100)}{\pi}\left[f\omega + \frac{(1-f)}{\omega}\right] > \frac{2\ln(100)}{\pi}, \tag{83}$$

the decay length is longer than that for a homogeneous isotropic strip and conversely. Inequality (83) holds under the following conditions:

$$f > \frac{1}{(1+\omega)} \quad \text{and} \quad \omega > 1, \tag{84}$$

or

$$f < \frac{1}{(1+\omega)} \quad \text{and} \quad \omega < 1. \tag{85}$$

This implies, for a given material, a geometric characterization of a structure which will satisfy (83). When $\omega > 1$, the material in the outer layers is stronger in shear in the z direction than is the core. In this case the decay length in the orthotropic two phase structure will be *greater* than that of the homogeneous isotropic structure if the orthotropic structure has a *thin*, i.e., $f > 0.5$, core. When $\omega < 1$, the same comparison holds if the orthotropic structure has a *thick*, i.e., $f < 0.5$, core.

Orthotropic two phase vs isotropic two phase. In comparing this orthotropic structure with the isotropic two phase structure, two main features are noted. First, the values of the characteristic material parameters $\omega = 1$ in the former and $\delta = 1$ in the latter each mark a transition point across which the effect of geometry on the decay length changes. Note that where $\omega = 1$ or $\delta = 1$, both problems reduce to that for an homogeneous isotropic strip.

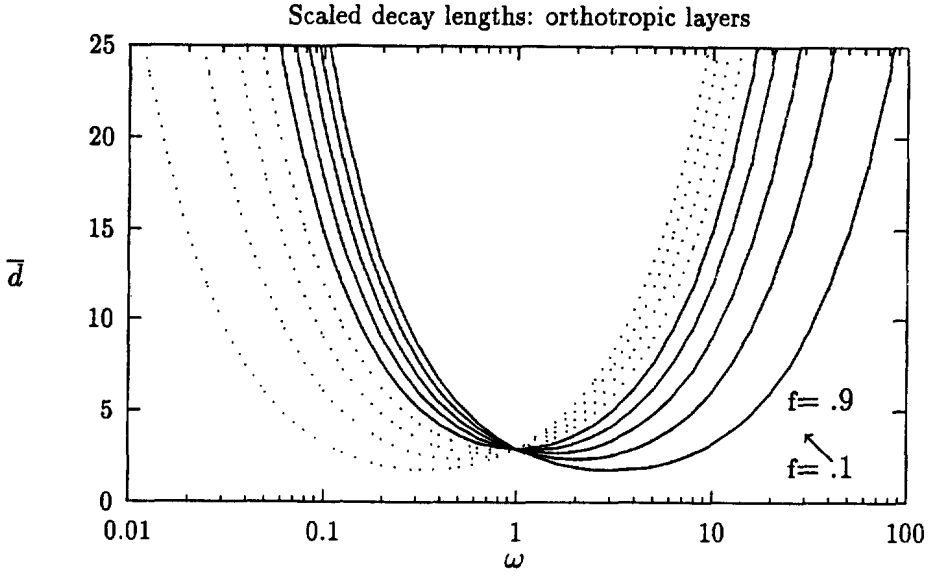

Fig. 7. Scaled decay length vs ω.

Second, a shorter decay length is achieved for the isotropic structure when the material parameters which characterize each layer μ_1, μ_2 are extremely different, whereas for this special orthotropic structure, the shorter decay lengths are found for materials where the values of G_{23}, G_{13} are close to one another. Figure 8 plots the scaled decay length as a surface over the values ω and f.

6.2. *Two distinct orthotropic phases*

The second illustrative example of a sandwich structure with orthotropic phases concerns numerical results for specific face and core materials. The data used here was supplied by W.B. Avery, Boeing Commercial Airplane Group, Seattle WA, and is used to indicate the order of magnitude which might be expected for the decay length in practical aircraft structures. The sandwich is composed of thin face layers of Hercules' AS4/8552 and Hexcel's HRP Honeycomb core. The elastic constants in the face ($a_{\alpha\beta}$) and core layers ($b_{\alpha\beta}$) are then

$$a_{11} = 153.2, \quad b_{11} = 6.3920, \tag{86}$$

$$a_{22} = 104.0, \quad b_{22} = 3.0456, \tag{87}$$

where all units are 10^4 psi. The geometry is defined by

$$2c_1 = 0.0876'', \quad 2c_2 = 0.75''. \tag{88}$$

From this data, one readily finds that

$$f = 0.1894, \ \gamma = 34.1476, \tag{89}$$

$$\hat{f} = 0.1638, \quad \hat{\delta} = 28.6082. \tag{90}$$

The first non-zero root of (57) is found to be

$$\lambda \doteq 0.4902. \tag{91}$$

From (31), the decay length is calculated as

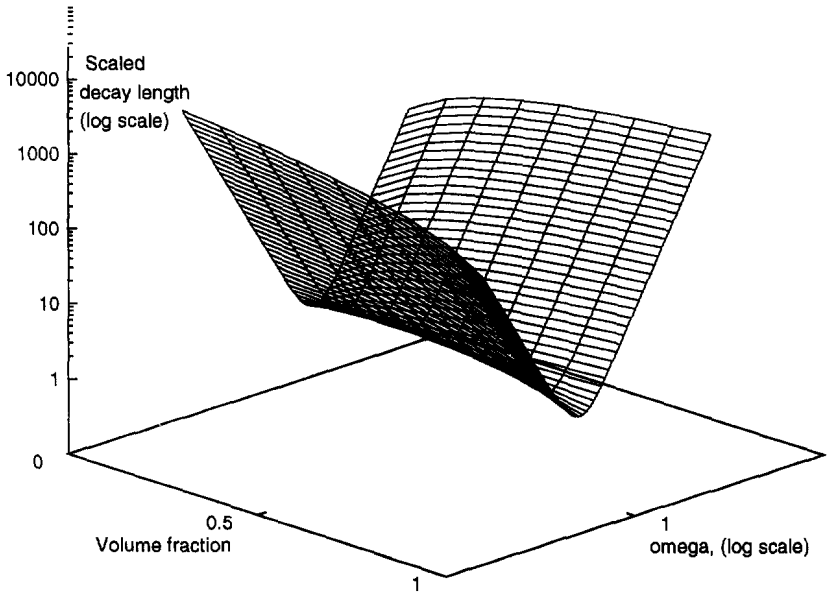

Fig. 8. Decay length surface: orthotropic [0/90/0] structure.

$$d \doteq 6.102''. \tag{92}$$

The corresponding result for a *homogeneous* isotropic strip is given by (30), (31), (36) as

$$d = \frac{2}{\pi}(2c_1 + c_2) \doteq 1.356''. \tag{93}$$

Thus the characteristic decay length (92) for the orthotropic sandwich structure is seen to be approximately four and a half times longer than that for the homogeneous isotropic strip. If the total width of the sandwich is denoted by h, then

$$d \doteq 6.5953\, h'', \tag{94}$$

while the characteristic decay length for the homogeneous isotropic strip is

$$d \doteq 1.4657\, h''. \tag{95}$$

7. CONCLUDING REMARKS

Previous research by Choi and Horgan (1978) on problems involving plane deformations of symmetric sandwich structures predicted a much longer decay length for Saint-Venant end effects in isotropic phase structures with relatively compliant cores compared with that for a homogeneous isotropic strip. The present work shows that similar conclusions can be reached regarding anti-plane shear deformations of isotropic phase structures. Additionally, it is found that an analogous result holds for isotropic phase structures where the conditions of perfect bonding are relaxed. The anti-plane shear deformation, with its simpler kinematics, allows for a more complete treatment of the Saint-Venant decay lengths, in particular with regard to asymptotic results for compliant and stiff cores respectively. Moreover, results for perfectly bonded sandwich strips with *anisotropic* phases have also been obtained.

Decay lengths for perfectly bonded isotropic two phase sandwich structures depend only on the two parameters f and δ defined in (32), (33) respectively. The first, f, the volume fraction, is a geometric parameter while δ, the core ratio, is a material parameter. For all geometries the decay length is an increasing function of the core ratio. The asymptotic estimate (39) accurately reflects this behavior for large values of δ. Recall that a large value of δ indicates a relatively compliant core. Moreover, (39) shows that the decay length tends to infinity as the core becomes infinitely compliant. Under conditions of imperfect bonding, this trend is maintained, i.e., longer decay lengths are obtained with increasing δ. This can also be observed, for finite values of δ, from the asymptotic formula (48) which is accurate for large values of the slip constant α.

Returning to the imperfect bonding case, some additional remarks can be made. The relaxation of the constraint of perfect bonding when modeling layered structures represents a more realistic physical model. It can account for the effect due to a thin layer of adhesive or differences in molecular structure at the interface due to the method of bonding. The presence of slip in the model results in an increase in the decay length. For large values of the slip parameter the decay length is so large that Saint-Venant's principle may be considered to fail. However, for small values of the slip parameter, the effects of boundary conditions, volume fraction and core ratio are similar to that of the perfect bonding model. In many cases the decay lengths are only slightly greater than those of the perfect bonding case, and the validity of Saint-Venant's principle is then judged by the same criteria as it is for perfect bonding. This suggests that the addition of small slip can more accurately reflect the physical behavior of the structure without fundamentally altering the decay of end effects.

In conclusion, it is of interest to compare the decay length for anti-plane shear deformations with that for plane deformations. For the homogeneous isotropic strip of width h, (31) and (37) yield

$$d \equiv d_{ap} = \frac{\ln(100)h}{\pi} \doteq 1.46h, \tag{96}$$

while it is well-known (see, e.g., Horgan and Knowles (1983), Horgan (1989)) that for plane strain or plane stress

$$d \equiv d_{ps} = \frac{\ln(100)h}{4.2} \doteq h. \tag{97}$$

Thus the decay length for anti-plane shear is *longer* than that for plane deformations in the case of a homogeneous isotropic strip. *Hence, in a combined loading situation, the anti-plane end effects penetrate further into the strip.* For the homogeneous anisotropic case, the situation is more complicated. For the class of anisotropy for which the anti-plane and plane deformation fields decouple, d_{ap} is given by (67) while d_{ps} depends on different elastic constants (see, e.g., Miller and Horgan (1995a, b)) and so a general comparison is not possible. For the symmetric sandwich structure, with isotropic phases, it has been shown in Section 3 that the material dependence of d_{ap} is reflected by the single parameter δ given in (33), whereas d_{ps} depends on two dimensionless material parameters, for example the Dundurs' parameters (see, e.g., Choi and Horgan (1978), Wijeyewickrema *et al.* (1996)). However, since (96), (97) show that in the limiting case of a homogeneous material

$$d_{ap} > d_{ps}, \tag{98}$$

one would expect (98) to hold also for sandwich structures with nearly identical phases.

Acknowledgements—This research was supported by the U.S. Air Force Office of Scientific Research under Grant AFOSR-F49620-95-1-0308, and by the U.S. Army Research Office under Grant DAAH04-94-G-0189. The research of S.C.B. was also supported by a grant from the Virginia Space Grant Consortium and an AASERT grant sponsored by the U.S. Army Research Office. We are grateful to Dr M. P. Nemeth, NASA Langley Research Center for several helpful discussions concerning this work. The authors are grateful to the reviewers for their constructive suggestions on an earlier draft of the manuscript.

REFERENCES

Aboudi, J. (1987). Damage in composites-modeling of imperfect bonding. *Comp. Sci. Tech.* **28,** 103–128.

Arimitsu, Y., Nishioka, K. and Senda, T. (1995). A study of Saint-Venant's principle for composite materials by means of internal stress fields. *J. Appl. Mech.* **62,** 53–58.

Baxter, S. C. (1995). Saint-Venant end effects for anti-plane shear deformations of sandwich structures. Ph.D. dissertation, University of Virginia.

Baxter, S. C. and Horgan, C. O. (1995). End effects for anti-plane shear deformations of sandwich structures. *J. Elast.* **40,** 123–164.

Benveniste, Y. (1984). On the effect of debonding on the overall behavior of composite materials. *Mech. of Mat.* **3,** 349–358.

Carlsson, L. A. and Pipes, R. B. (1987). *Experimental Characterization of Advanced Composite Materials*, Prentice-Hall, Englewood Cliffs, N.J.

Choi, I. and Horgan, C. O. (1977). Saint-Venant's principle and end effects in anisotropic elasticity. *J. Appl. Mech.* **44,** 424–430.

Choi, I. and Horgan, C. O. (1978). Saint-Venant end effects for plane deformation of sandwich strips. *Int. J. Solids Structures* **14,** 187–195.

Crafter, E. C., Heise, R. M., Horgan, C. O. and Simmonds, J. G. (1993). The eigenvalues for a self-equilibrated semi-infinite, anisotropic elastic strip. *J. Appl. Mech.* **60,** 276–281.

Devries, F. (1993). Bounds on elastic moduli of unidirectional composites with imperfect bonding. *Comp. Engng* **3,** 349–382.

Gibson, R. F. (1994). *Principles of Composite Material Mechanics*, McGraw-Hill, New York.

Horgan, C. O. (1982). Saint-Venant end effects in composites. *J. Comp. Mat.* **16,** 411–422.

Horgan, C. O. and Knowles, J. K. (1983). Recent developments concerning Saint-Venant's principle. *Advances in Applied Mechanics*, Vol. 23 (eds J. W. Hutchinson and T. Y. Wu), pp. 179–269, Academic Press, New York.

Horgan, C. O. (1989) Recent developments concerning Saint-Venant's principle: an update. *Appl. Mech. Rev.* **42,** 295–303.

Horgan, C. O. and Payne, L. E. (1993). On the asymptotic behavior of solutions of linear second-order boundary-value problems on a semi-infinite strip. *Archive Rational Mech. Anal.* **124,** 277–303.

Horgan, C. O. and Miller, K. L. (1994). Anti-plane shear deformations for homogeneous and inhomogeneous anisotropic linearly elastic solids. *J. Appl. Mech.* **61,** 23–29.

Horgan, C. O. and Simmonds, J. G. (1994). Saint-Venant end effects in composite structures. *Comp. Engng* **3,** 279–286.

Horgan, C. O. (1995). Anti-plane shear deformations in linear and nonlinear solid mechanics. *SIAM Rev.* **37,** 53–81.

Miller, K. L. and Horgan, C. O. (1995a). End effects for plane deformations of an elastic anisotropic semi-infinite strip. *J. Elasticity* **38,** 261–316.

Miller, K. L. and Horgan, C. O. (1995b). Saint-Venant end effects for plane deformations of elastic composites. *Mech. Comp. Mat. Structures* **2,** 203–214.

Wijeyewickrema, A. C. and Keer, L. M. (1994). Axial decay of stresses in a layered composite with slipping interfaces. *Comp. Engng* **4,** 895–899.

Wijeyewickrema, A. C. (1995). Decay of stresses induced by self-equilibrated end loads in a multilayered composite. *Int. J. Solids Structures* **32,** 515–523.

Wijeyewickrema, A. C., Horgan, C. O. and Dundurs, J. (1996). Further analysis of end effects for plane deformations of sandwich strips. *Int. J. Solids Structures* **33,** 4327–4336.